JOURNAL OF COMPUTATIONAL PHYSICS 39, 179–200 (1981)

A Numerical Method for Two Phase Flow with an Unstable Interface

J. GLIMM*,† AND D. MARCHESIN†,||

The Rockefeller University, New York, New York 10021

AND

O. MCBRYAN‡,§,#

Courant Institute, New York University, New York, New York 10012

The random choice method is used to compute the oil–water interface for two dimensional porous media equations. The equations used are a pair of coupled equations: the (elliptic) pressure equation and the (hyperbolic) saturation equation. The equations do not include the dispersive capillary pressure term and the computation does not introduce numerical diffusion. The method resolves saturation discontinuities sharply. The main conclusion of this paper is that the random choice is a correct numerical procedure for this problem even in the highly fingered case. Two methods of inducing fingers are considered: deterministically, through choice of Cauchy data and heterogeneity, through maximizing the randomness of the random choice method.

1. INTRODUCTION

The equations of two phase immiscible flow in porous media have the form

$$\frac{\partial s}{\partial t} + \nabla \cdot (\mathbf{v} f(s)) = 0, \tag{1.1}$$

$$\mathbf{v} = -k(s)\,\nabla p, \tag{1.2}$$

$$\nabla \cdot \mathbf{v} = 0, \tag{1.3}$$

neglecting the dispersive, or parabolic term associated with capillary pressure. Here s denotes the saturation (fraction of water in total fluid) and p is pressure. Also k and f

* Supported in part by NSF Grant PHY-78-08066.
† Supported in part by the Army Research Office, ARO Grant DAAG29-78-G-0171.
‡ Supported in part by NSF Grant DMR 77-04105.
§ Permanent address: Mathematics Department, Cornell University, Ithaca, N.Y.
|| Permanent address: Mathematics Department, Pontificia Universidade Catolica do Rio de Janeiro, Rio de Janeiro, Brazil.
Supported in part by the Department of Energy, Grant EY-76-C-02-3077.

0021-9991/81/010179–22$02.00/0

are known functions of saturation (and perhaps position), which describe the permeability and porosity of the reservoir and the viscosities of the two incompressible phases flowing in it. We use the functions

$$k(s) = s^2 + (1-s)^2/\mu, \tag{1.4}$$

$$f(s) = s^2/k(s), \tag{1.5}$$

where μ is the viscosity ratio for the fluids in question. In order to eliminate geometrical effects from the study of viscous fingering, we have chosen as a model geometry a rectangle $0 \leqslant x \leqslant X$, $0 \leqslant y \leqslant Y$, and with the boundary conditions

$$\begin{gathered} s(x, y=0, t) = s_0(x), \\ \partial_x p(x=0, y, t) = \partial_x p(x=X, y, t) = 0, \\ p(x, y=0, t) = 0, \qquad p(x, y=Y, t) = -vY. \end{gathered} \tag{1.6}$$

This problem is intrisically one dimensional. Except for fingering instabilities (the central point of this paper) the solutions would be one dimensional also. Elsewhere we present calculations in which the underlying flow is intrinsically two dimensional [10, 19].

We have fixed $v = 1$ throughout this paper. This is no loss of generality because change of v is equivalent to change of time scale. In most cases we have chosen $s_0(x) = 1$. This corresponds to a situation where water is injected at one edge ($y = 0$) of the rectangle and fluid is removed at the opposite edge in such a way that a fixed pressure difference is maintained. Initial data are also specified, usually $s = 0$ at interior points.

Problem (1.1)–(1.6) is scale invariant. This means that for any $a > 0$,

$$\begin{aligned} s'(x, t) &= s(ax, at), \\ p'(x, t) &= a^{-1} p(ax, at), \end{aligned} \tag{1.7}$$

solves (1.1)–(1.6) in the rectangle $0 \leqslant x \leqslant X' = a^{-1}X$, $0 \leqslant y \leqslant Y' = a^{-1}Y$ if s, p solves (1.1)–(1.6) in $[0, X] \times [0, Y]$.

The porosity and absolute permeability (assuming for the moment that they have no spatial variations) scale out of Eqs. (1.1)–(1.3) (see (1.7)) and thus these factors have been set to one for convenience. In general, reservoirs are not spatially homogeneous, and in this sense Eqs. (1.1)–(1.3) do not correctly model all of their important properties. In some cases, information concerning the long distance variation, or trend, is known from geological data. This type of heterogeneity is most important in realistic field applications. Here and in [9, 10] we consider problems in which such trends do not occur.

Geological information concerning horizontal variation on distances between one quarter of a mile—the typical well spacing—and six inches—a core diameter—is not abundant, but it seems to be widely assumed that significant variation occurs on all

intermediate length scales. Furthermore, the variation continues on all length scales down to the smallest pore size. We have chosen in [9, 10] a numerical procedure consistent with this picture of a reservoir which is heterogeneous on small length scales (i.e., on the order of a mesh spacing).

The present paper, in addition to showing sample heterogeneous calculations, in both the stable and unstable cases, validates the correct propagation of these fingers by the use of totally deterministic calculations.

Because there are many significant length scales in the problem, including those well below the level of our mesh spacing, one may worry about the meaning of the computations. However, there is a cutoff on the relevance of short length scale heterogeneity effects. This cutoff is provided by capillary pressure effects, and is between several inches and several hundred feet, depending on the reservoir, the flooding process and the point (x, y) where the question is asked.

The dispersive effects produced by a capillary pressure term are not included in the scale invariant equations (1.1)–(1.3). Thus, when solving these equations numerically for finger-like solutions it is meaningless to consider mesh refinement beyond the level of the capillary cutoff. In the present computations we imagine that our mesh spacing is set at this "mixing zone" length scale. If we were to solve the physical problem using finer meshes, a parabolic term should be included in (1.1), simulating the capillary pressure effect. This parabolic term would stabilize the solution, in the sense that the smallest fingering instabilities would have the correct size.

We are interested in determining the oil–water saturation front, for values of μ corresponding to both stable and unstable (fingering) regimes. Since the detailed information concerning the specific x–y dependence of the permeability (and porosity) is not contained in (1.1)–(1.3), if the method is to have any relevance to engineering reality, the problem must be considered to be stochastic in nature, with fluctuations larger than infinitesimal. Thus the solution is stochastic also. Some important aspects of the stochastic solution, however, are deterministic, at least as far as our tests reveal in [9]. Specifically, the growth rate of fingers, in the unstable case appears to be deterministic.

Since we included in the formulation of the problem the assumption that non-infinitesimal deviations from homogeneity are important, we are not attempting to model the onset of instability. For the latter purpose, one might include a deterministic response to a single perturbation, e.g., a sine wave with the lowest nonzero frequency determined by the dimensions of the region. Calculations of the onset of instability occur in many numerical studies of boundary layers, mixing layers, heat, convection, etc. We are concerned with a highly developed instability: the number of unstable modes is of the order of the number of mesh intervals in the width of the region. Our calculations are thus closer in spirit to the study of fully developed turbulence than, say, to the study of the onset of turbulence. We note in passing that for the problem of onset of instabilities a linearized analysis is relevant. The latter question is discussed in the book of Scheidegger [16], where a list of further references can be obtained.

In [9] we computed statistical quantities, and found that these quantities are deter-

ministic in the sense that they are independent of mesh refinement, choice of random number generator, scale transformation and boundary effects of the rectangular domain.

In the present paper we try to justify the use of our numerical procedure in computing stable and unstable (fingered) solutions.

We show that the method is reasonably well conditioned under mesh refinement. In a particular fingered case where an approximate solution can be computed explicitly, we show that the numerical procedure yields results accurate within expected error bounds. This example is also used to discuss the mechanism responsible for the growth of non-infinitesimal fingers.

We also show that in the stable regime (small values of μ) the randomness introduced in [9] to generate the fingers does not spoil the stability of the solution. In other words, fingers do not develop.

The closely related problem of computing unstable fingering in the case of miscible displacement was previously considered by Peaceman and Rachford [13]. We also mention the related problems of salt fingering in the ocean and flame front fingers.

2. The Numerical Procedure

The basic quantities at time t_n ($n = 0, 1, 2, 3,...$) are the velocity $\{\mathbf{v}^n_{i+1/2,j+1/2}\}$ and the saturation $\{s^n_{i+1/2,j+1/2}\}$ computed at the center of mesh blocks, and the pressure $\{p^n_{i,j}\}$, computed at mesh points, ($0 \leqslant i \leqslant N$, $0 \leqslant j \leqslant M$)—see Fig. 1. Note that i labels mesh units in the x direction and j labels mesh units in the y direction.

At time zero, the saturation $\{s^0_{i+1/2,j+1/2}\}$ is the given Cauchy data. (We frequently use saturation zero everywhere except at the $j = 0$ row where it is one. This corresponds to water starting to seep in from the $j = 0$ side of the rectangular oil reservoir.)

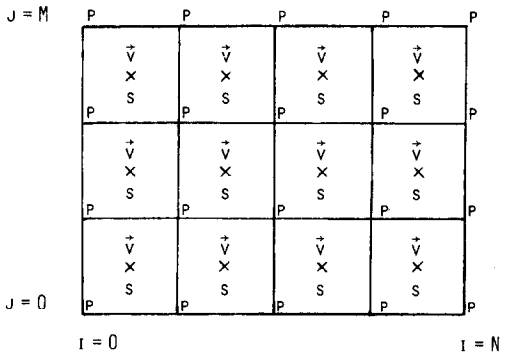

FIG. 1. The grid: pressure, velocity and saturation.

The solution is advanced from time t_{n-1} to time t_n through the following steps:

(A) Given the saturation $\{s^{n-1}_{i+1/2,j+1/2}\}$, we solve (1.3) approximately obtaining $\{p^n_{i,j}\}$.

(B) The velocity $\{\mathbf{v}^n_{i+1/2,j+1/2}\}$ is obtained using a discrete version of (1.2).

(C) Equation (1.1) is solved approximately for the saturation $\{s^n_{i+1/2,j+1/2}\}$.

This procedure is first order in time and space. We describe each of its steps in detail.

A. *The Elliptic Equation*

We are given the saturation $\{s_{i+1/2,j+1/2}\}$ and we want to solve approximately the elliptic equation (1.3) under the boundary conditions (1.6).

We introduce a new function

$$\phi(x, y) = p(x, y) + vy.$$

Equations (1.3) and (1.6) may be rewritten as

$$-\nabla \cdot (k \nabla \phi) + v \frac{\partial k}{\partial y} = 0, \tag{2.1}$$

$$\frac{\partial \phi}{\partial x}(0, y) = \frac{\partial \phi}{\partial x}(X, y) = 0, \tag{2.2a}$$

$$\phi(x, 0) = \phi(x, Y) = 0. \tag{2.2b}$$

Using standard finite element techniques [17], this problem is reduced to the solution of a linear system. We approximate the solution ϕ by a continuous function, piecewise linear in triangles (halves of mesh blocks). We obtain the following system:

$$A_{i,j}\phi_{i,j} + B_{i,j}\phi_{i+1,j} + C_{i,j}\phi_{i-1,j} + D_{i,j}\phi_{i,j+1} + E_{ij}\phi_{i,j-1} = F_{i,j}$$
$$i = 0,..., N; \quad j = 1,..., M-1; \tag{2.3}$$

where

$$A_{ij} = (1/2)((\Delta x)^{-2} + (\Delta y)^{-2})(k_{i+1/2,j+1/2} + k_{i+1/2,j-1/2} + k_{i-1/2,j-1/2} + k_{i-1/2,j+1/2}), \tag{2.4a}$$

$$B_{ij} = -(1/2)(\Delta x)^{-2}(k_{i+1/2,j+1/2} + k_{i+1/2,j-1/2}), \tag{2.4b}$$

$$C_{ij} = -(1/2)(\Delta x)^{-2}(k_{i-1/2,j+1/2} + k_{i-1/2,j-1/2}), \tag{2.4c}$$

$$D_{ij} = -(1/2)(\Delta y)^{-2}(k_{i-1/2,j+1/2} + k_{i+1/2,j+1/2}), \tag{2.4d}$$

$$E_{ij} = -(1/2)(\Delta y)^{-2}(k_{i-1/2,j-1/2} + k_{i-1/2,j-1/2}), \tag{2.4e}$$

$$F_{ij} = (v/2)(\Delta y)^{-1}(k_{i-1/2,j-1/2} - k_{i-1/2,j+1/2} + k_{i+1/2,j-1/2} - k_{i+1/2,j+1/2}). \tag{2.4f}$$

In the formulae above $k_{i\pm 1/2,j\pm 1/2} = k(s_{i\pm 1/2,j\pm 1/2})$ unless the point corresponding to $i \pm 1/2, j \pm 1/2$ falls out of the rectangular domain. In this case $k_{i\pm 1/2,j\pm 1/2}$ should be

replaced by zero. Note that for $\Delta x = \Delta y = 1$, and $k(s) \equiv 1$, the formulae above reduce to the usual $4, -1, -1, -1, -1$ coefficients of the Laplacian, except at the left and right boundary points, where the coefficients are $3, -1, -1, -1$.

An accelerated conjugate gradient algorithm was used to solve this system. (See Appendix A.) It is a pleasure to thank O. Widlund for helpful discussions. We remind the reader that a preconditioning operator is an approximation of the operator on the left hand side of (2.3), which must be symmetric positive definite and easy to invert. We experimented with three operators as preconditioning.

The first operator, which we call $\mathscr{D}$, is the diagonal part of the left hand side of (2.3), namely,

$$(\mathscr{D}\phi)_{ij} = A_{ij}\phi_{ij}. \tag{2.5}$$

The second operator is $\mathscr{D}^{1/2}\mathscr{L}\mathscr{D}^{1/2}$ where $\mathscr{L}$ is the usual approximation to the operator $-\Delta$ with appropriate boundary conditions on the mesh in consideration. Standard techniques involving fast Fourier transforms were used to apply $\mathscr{L}^{-1}$ to vectors in the accelerated conjugate gradient procedure.

The third operator was

$$\mathscr{D}^{1/2}(m + \mathscr{L}_x)(m + \mathscr{L}_y)\mathscr{D}^{1/2}, \tag{2.6}$$

where m is a positive member (of order one), and $\mathscr{L}_x$ and $\mathscr{L}_y$ are usual approximations to $-\partial^2/\partial x^2$ and $-\partial^2/\partial y^2$ with appropriate boundary conditions. Inverting $(m + \mathscr{L}_x)$ and $(m + \mathscr{L}_y)$ is very cheap because it involves solving tridiagonal systems with constant coefficients. Even though the number of iterations needed for convergence in the accelerated conjugate gradient was perhaps four of five times smaller when using the second preconditioning rather than the third, the latter turned out to be the cheapest in our applications. Undoubtedly this is mainly due to the simplicity of inverting the third operator. We conjecture that another factor is the strongly fingered structure of most of our solutions. They have Fourier modes which are concentrated on high frequencies in the x direction and on low frequencies in the y direction, justifying the splitting in the third operator. We remark that this preconditioning is closely related to a splitting method used by Peaceman and Rachford [14].

Typically the iteration in the accelerated conjugate gradient is stopped when the residual error is 10^{-3} times smaller than the norm of the solution itself. As an initial guess in the procedure, we use the solution at the previous time step.

B. *The Velocity Equation*

The formula used to compute the velocity

$$v^n_{i+1/2,j+1/2} \equiv (u^n_{i+1/2,j+1/2}, w^n_{i+1/2,j+1/2}),$$

is

$$u^n_{i+1/2,j+1/2} = -k(s^{n-1}_{i+1/2,j+1/2})[(p^n_{i+1,j+1} - p^n_{i,j+1}) + (p^n_{i+1,j} - p^n_{i,j})]/2 \tag{2.7}$$

with a similar formula for $w^n_{i+1/2,j+1/2}$. They can be easily derived by integrating the velocity $\mathbf{v} = -k\nabla p$ on a mesh block. (We take p as given by its finite element approximation.)

These formulas are satisfactory in the region where the velocity is continuous. The normal component of the velocity is still computed accurately at fronts which are parallel to the grid. This is so because this component is continuous, as implied by Eq. (1.3). On the other hand, the normal component is the only one which affects the motion of the front, as can be seen from $\partial s/\partial t + \mathbf{v}\cdot\nabla f(s) = 0$. (This equation is obtained by adding (1.1) and (1.3).)

Finally, we remark that the fronts in our solution are essentially parallel to the grid, in one or the other direction. Thus we believe that the formulas for the velocity give satisfactory results in the cases where they are used.

C. *The Hyperbolic Equation*

We use the random choice method [7, 2] to advance the solution of the Buckley–Leverett equation (1.1) from time t_{n-1} to time t_n. This method was first used to solve this equation in [1, 5]. Since it is an intrinsically one dimensional method, operator splitting is used, i.e., a time step for the equation

$$s_t + \frac{\partial}{\partial x}(uf(s)) + \frac{\partial}{\partial y}(wf(s)) = 0 \tag{2.8}$$

is replaced by a time step of

$$s_t + \frac{\partial}{\partial y}(wf(s)) = 0, \tag{2.9}$$

followed by a time step of

$$s_t + \frac{\partial}{\partial x}(u(f(s)) = 0. \tag{2.10}$$

The boundary conditions (1.6) for (2.8) are replaced by $s(x, y = 0, t) = s_0(x)$.

This is an adequate first order procedure for smooth flows [18]. In general, it tends to degrade the resolution of discontinuity fronts which are oblique to the grid [3]. However, this problem is substantially reduced in our case, since the velocity field is essentially one dimensional (typically the x component of the velocity is between 10^{-2} and 10^{-1} the size of the y component). In practice the x component hyperbolic timestep, of the operator splitting produces no motion most of the time. Furthermore, the fingered solutions we consider in this paper have fronts which are mainly parallel to the grid, either in the x or the y direction (see Section 3). For these solutions the use of operator splitting is allowed: since only the normal component of the velocity is responsible for the motion of the fronts, Eq. (2.8) reduces locally to (2.9) or (2.10).

The one-step version of the random choice method employed is found in [8]. We give a brief description of the method for Eq. (2.10). (For each value of j, Eq. (2.10) is a one dimensional problem, so we drop the index j.) At time t_{n-1}, the solution is

assumed to be the constant $s^{n-1}_{i+1/2}$ in the interval $i\,\Delta x \leqslant x < (i+1)\,\Delta x$, for $i = 0, 1, 2, \ldots, N-1$. Similarly we define velocities constant in intervals $(i-1/2)\,\Delta x \leqslant x < (i+1/2)\,\Delta x$, $i = 1, 2, \ldots, N-1$, by the formula $\tilde{u}^n_i = (u^n_{i-1/2} + u^n_{i+1/2})/2$. For $t_{n-1} \leqslant t < t_{n-1} + \Delta t$, when a Courant–Friedrichs–Levy type condition $\Delta t \leqslant \frac{1}{2}\,\Delta x(\sup_i \tilde{u}^n_i) \times (\sup_s f'(s))$ is obeyed, the solution is uniquely defined. The factor $\frac{1}{2}$ results from our use of a nonstaggered mesh and allowance for wave motion in either direction. The solution is obtained by solving the following Riemann problems (for each i)

$$s_t + \frac{\partial}{\partial x}(\tilde{u}_i f(s)) = 0,$$

$$s = s^{n-1}_{i-1/2}, \qquad \text{for} \quad x < i\,\Delta x, \quad t = t_{n-1}$$

$$s = s^{n-1}_{i+1/2}, \qquad \text{for} \quad x > i\,\Delta x, \quad t = t_{n-1}$$

$$\tilde{u}_i = (u^n_{i-1/2} + u^n_{i+1/2})/2.$$

The solution of the Riemann problem follows [5]. Thus a solution $s(x, t)$ is obtained for $t_{n-1} \leqslant t < t_{n-1} + \Delta t \equiv t_n$; this solution is not piecewise constant in this time interval. To achieve the latter property, we modify s at $t = t_n$. We introduce a sequence $\{\theta_n\}$ of numbers equidistributed in the interval $[0, 1]$. (In this paper we use the fractional part of $((n + \text{const.})\sqrt{2}.)$ Finally we define

$$s^n_{i+1/2} = s((i + \theta_n)\,\Delta x, t_n), \qquad i = 0, 1, 2, \ldots, N-1.$$

In this method, each wave in the solution achieves its correct speed statistically (as in a random walk) but because adjacent fluid blocks are never averaged or mixed, numerical diffusion is completely eliminated. A detailed discussion of this method can be found, e.g., in [3, 5, 11].

The averaging formula which defines u^n_i is justified at the fronts if we remember that the normal component of the velocity is continuous and that we are mostly concerned with fronts which are parallel to the grid.

In practice the time step used from t_{n-1} to t_n was obtained by extrapolation: namely computation of a maximum allowed time step from the solution of the Riemann problems in the x and y directions at time t_{n-2}. This maximum allowed time step was then reduced by a factor (10 % in these calculations) to allow for time dependence of the maximum allowed time step. For the first time step the hyperbolic equation is solved once for a very short time step in order to estimate the correct length for the first time step.

3. Results

A. *The Single Finger: Homogeneous Calculations*

As Cauchy data we use a flat front of water, except for a protruding finger, and we follow its development in time. This is done for $\mu = 4$, when the oil-water front is

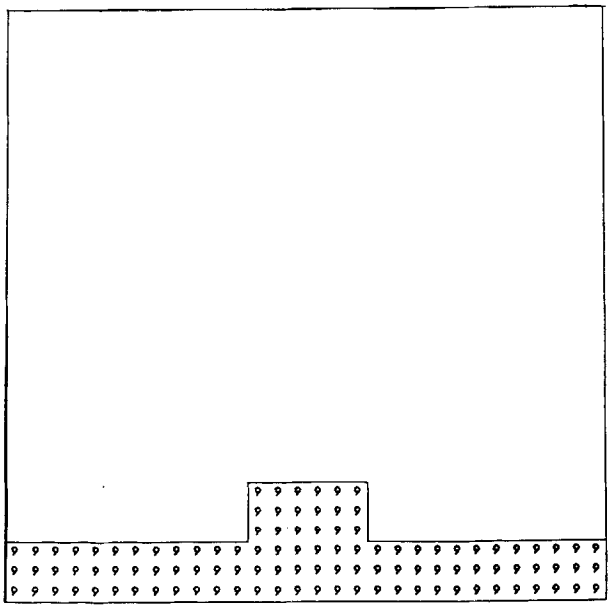

FIG. 2. Cauchy data for Figs. 3–7: Saturation values. Here 9 represents pure water, i.e., $s = 1$. The zeros (pure oil) are not printed.

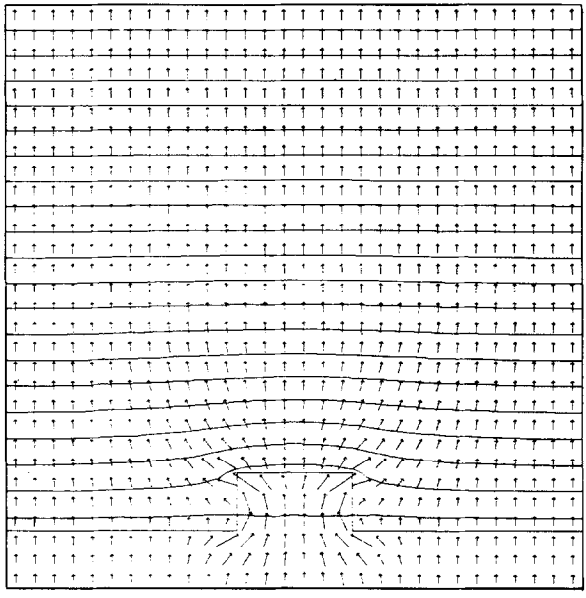

FIG. 3. Pressure level lines and velocity field at time zero. The horizontal velocities are exaggerated by a factor of five relative to vertical velocities in all graphs.

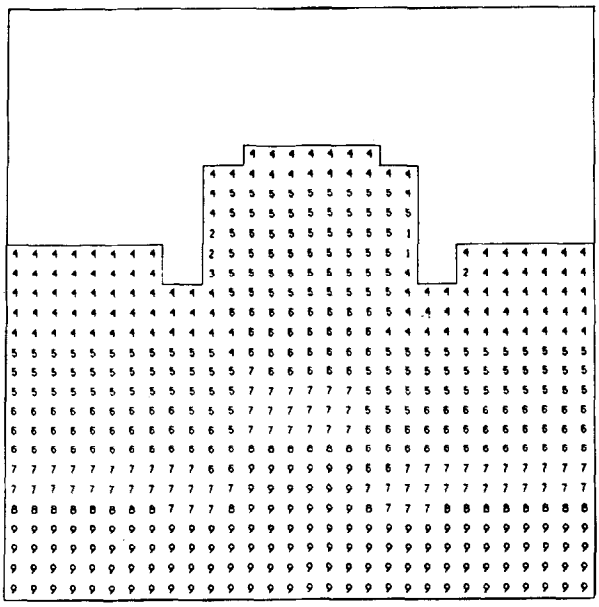

FIG. 4. Saturation value at time $t = 1$ on a 30×30 grid.

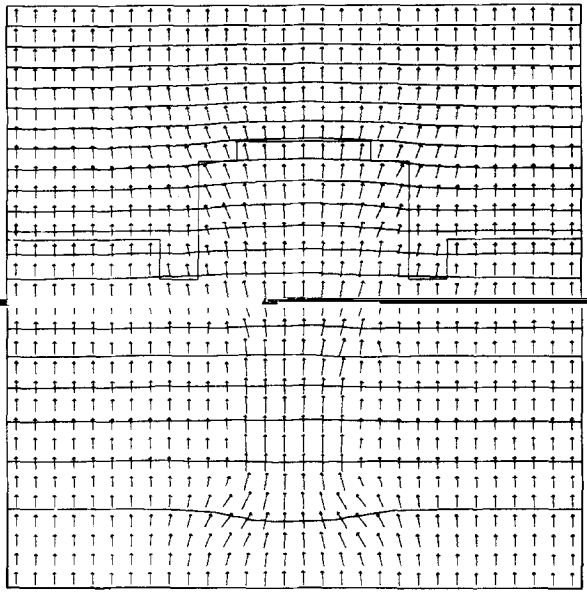

FIG. 5. Pressure contour lines and velocity field at time $t = 1$ on a 30×30 grid. The saturation front is superimposed.

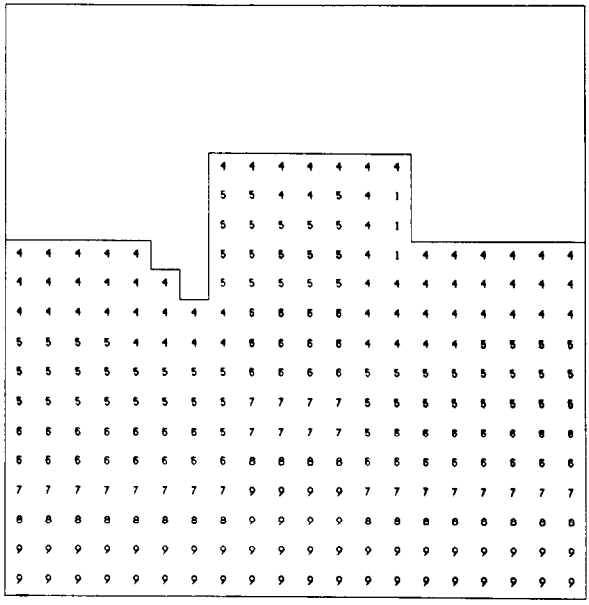

FIG. 6. Saturation value at time $t = 1$ on a 20×20 grid. See Fig. 4 for effect of mesh refinement.

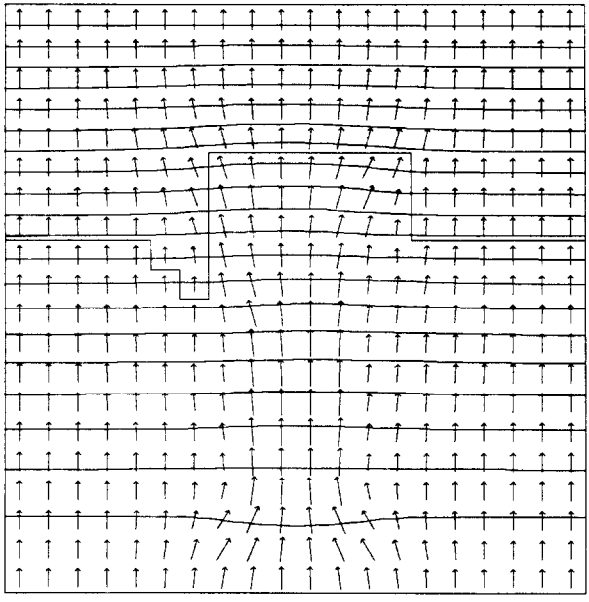

FIG. 7. Pressure contour lines and velocity field at time $t = 1$ on a 20×20 grid. See Fig. 5 for effect of mesh refinement. Velocity arrows are scaled by length of mesh spacing.

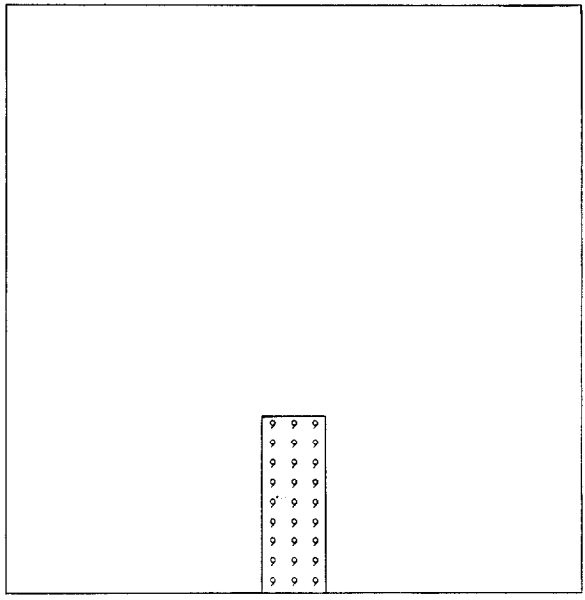

FIG. 8. Cauchy data for Figs. 9–15: Saturation values (29 × 30 mesh).

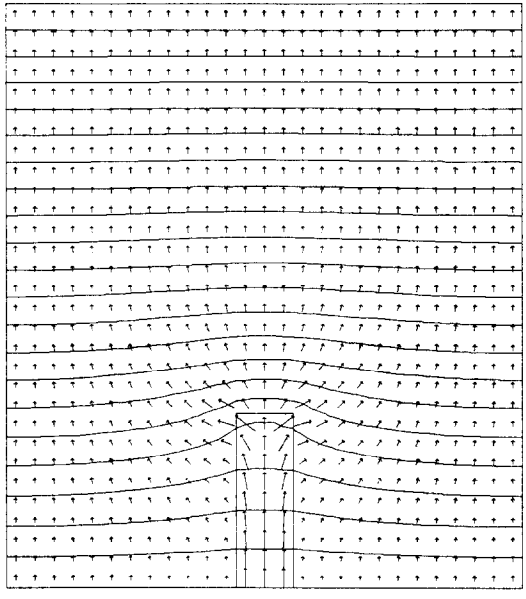

FIG. 9. Pressure contour lines and velocity field at time zero (29 × 30 mesh).

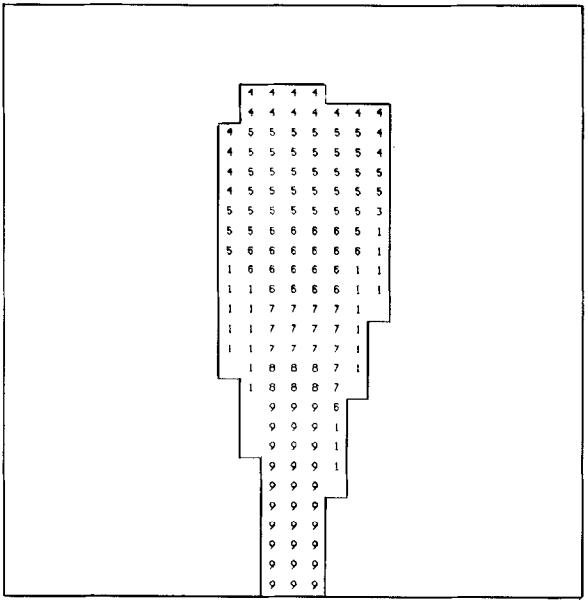

FIG. 10. Saturation values at $t = 1$. The apparent loss of resolution (0's and 1's) of the front on the trailing edge above the base of the finger is a physical effect. It is a residue of water left in a region where oil displaces water (29 × 30 mesh).

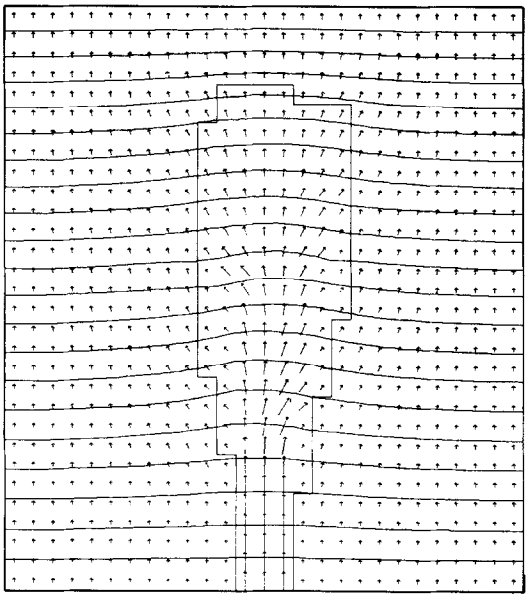

FIG. 11. Pressure contour lines and velocity field for Fig. 10 (29 × 30 mesh).

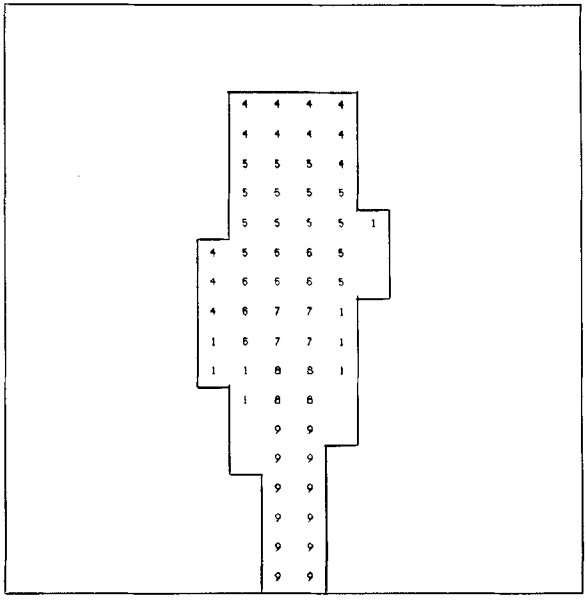

FIG. 12. Medium mesh (19 × 20) saturation values at time $t = 1$, compare to Fig. 10.

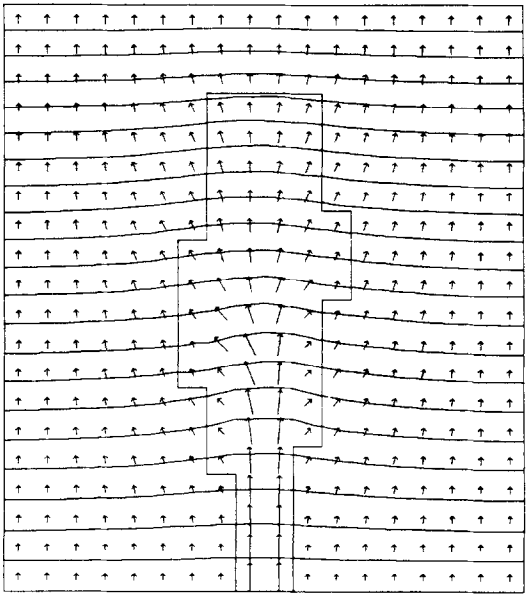

FIG. 13. Pressure contour lines and velocity field for Fig. 12 (19 × 20 mesh).

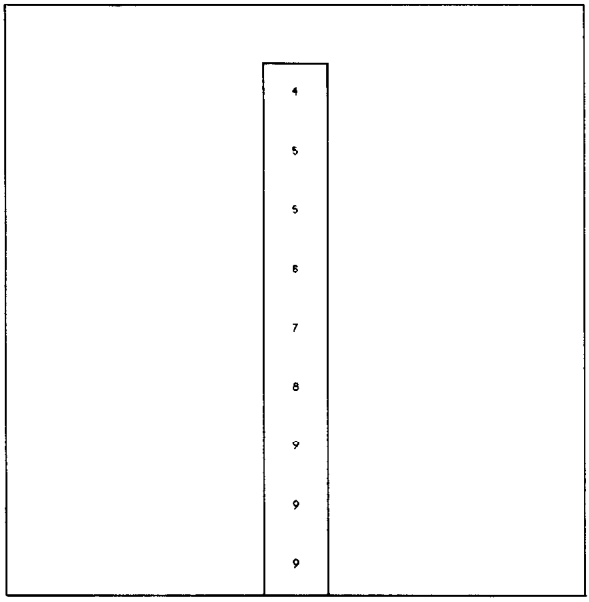

FIG. 14. Coarse mesh (9×10) saturation values at time $t = 1$. Compare to Figs. 10, 12.

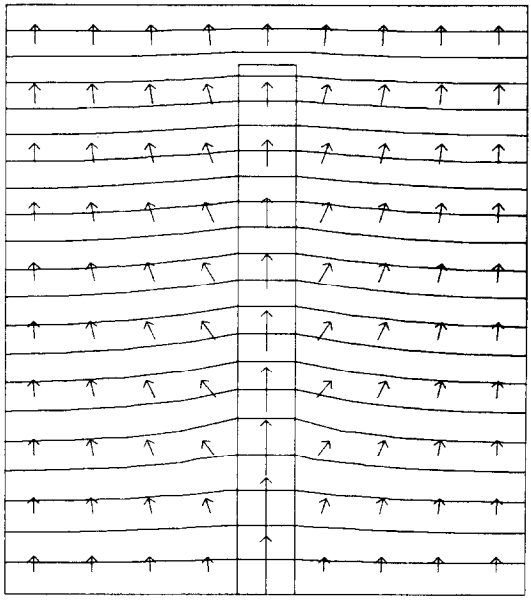

FIG. 15. Pressure contour lines and velocity field for Fig. 14.

unstable. (As explained later, this means that fingers tend to form from an initially smooth interface).

In Figs. 2–7, we display the evolution of a thick finger, both for a fine (30×30) grid and medium grid (20×20). The numbers 0,..., 9 correspond to saturation varying from $s = 0$ (pure oil) to $s = 1$ (pure water). (Actually the number 0 is not printed in the plots.) The front is drawn at height $s = 0.01$, which tends to make the results look worse by accentuating any dispersion. For plotting convenience the velocity scales are not the same for different grids. (Actual inspection of the numbers shows that the velocities for different grids agree well.) For clarity, the horizontal component of the velocity is multiplied by five in all the plots. We have good agreement under mesh refinement.

In Figs. 8–15 we display the evolution of a thin finger, for a fine (30×30) grid, a medium (20×20) grid and a coarse (10×10) grid. Within the accuracy of the scheme, we have good agreement under mesh refinement, particularly as far as the length of the finger is concerned.

B. *The Initially Constant Front: Heterogeneous Calculations*

We consider now the situation when $s_0(x) = 1$ in (1.6). The problem we are solving has no x dependence, so its mathematical solution is independent of x and may be found by the method of lines. Since $\nabla \cdot \mathbf{v} = 0$ and $\mathbf{v} = (0, w)$, w is constant. Using $\mathbf{v} = -k \nabla p$ and the boundary condition (1.6) we obtain $w = vY / \int_0^Y (k(s))^{-1} \, dy$. If we let $\tau = t/w$, the hyperbolic equation becomes $s_\tau + f(s)_y = 0$. Typically the solution as a function of y has the form shown in Figs. 16 and 17. However, this solution is unstable for μ sufficiently large, and the solutions of physical interest are those which

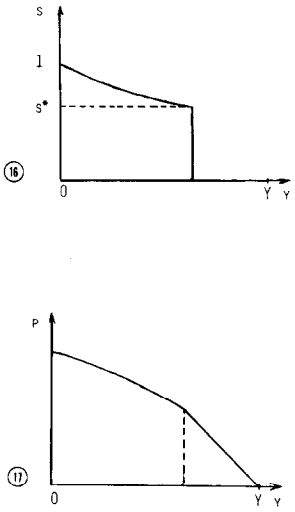

FIGS. 16–17. Saturation and pressure. Solution of the one dimensional flow problem for a typical time t.

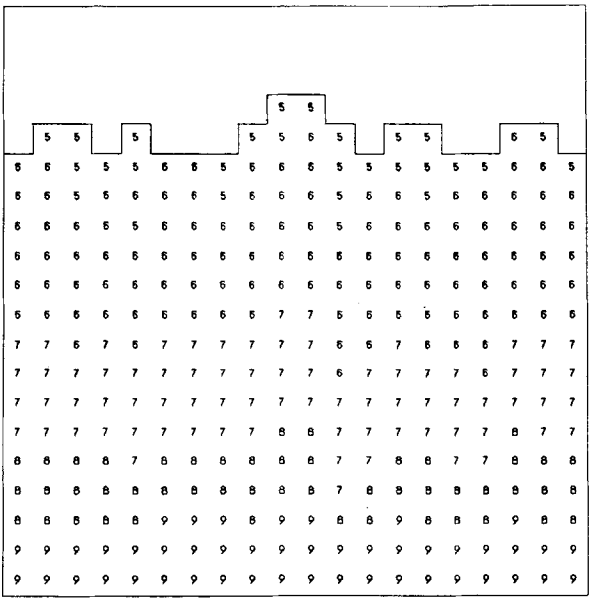

FIG. 18. Saturation values at $t = 2$ for full x–y heterogeneous calculation. Initial data were $s = 1$ for $y = 0$. The viscosity ratio $\mu = 2$ is stable and the front is within one mesh spacing of its mean position. This variation in the front is due to statistical effects, introduced here numerically.

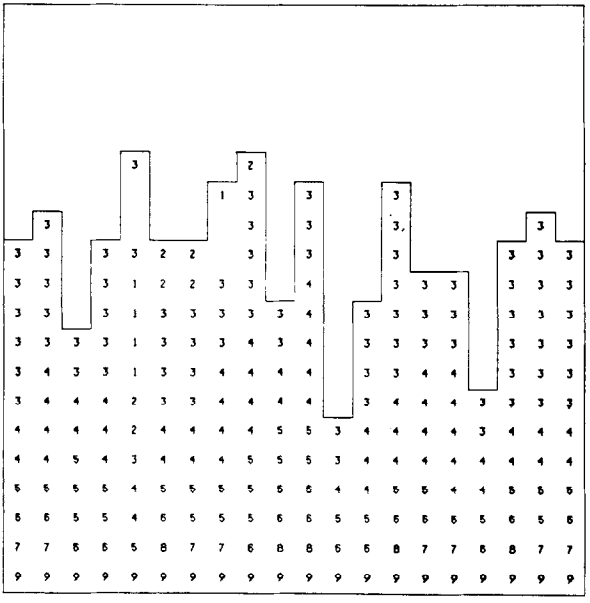

FIG. 19. Saturation values at $t = 2$ in the unstable case, $\mu = 10$, for a full x–y heterogeneous calculation. The 0's, 1's and 2's behind the front are partly physical: due to pinching behind a narrow finger, the resulting isolated droplet leaves a narrow trail of water. (Initial data were $s = 1$ for $y = 0$.)

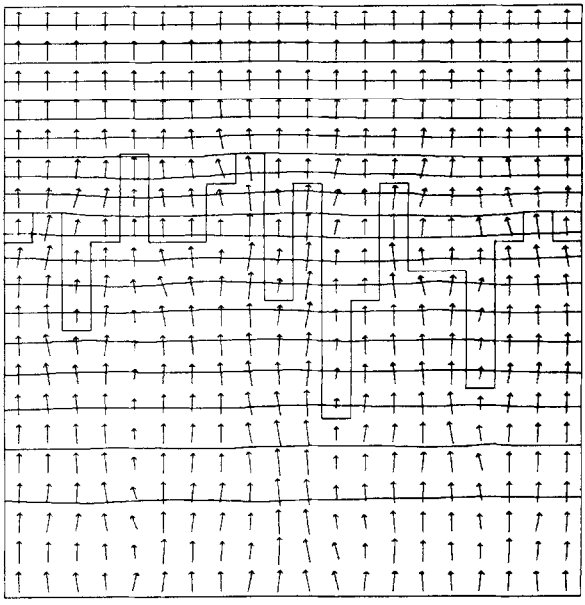

FIG. 20. Pressure contour lines and velocity field for Fig. 19 (20×20 grid).

result from small (x-dependent) perturbations of the data. Here the randomness of the random choice method is an advantage, because it can be used to introduce small random perturbations into the solution at each time step. In the stable region, $u < u_c$, these small perturbations are damped out and do not affect the solution

sense, the random choice method can be thought of as simulating a slightly heterogeneous medium. In the present paper, we have no control over the degree of heterogeneity except that we choose distinct random number generators for each column $x = \text{const.}$ in the mesh. This is achieved by choosing the constant in

$$\theta_n \equiv (n + \text{constant})\sqrt{2} (\text{mod } 1)$$

to depend on x.

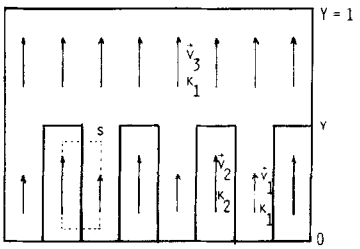

FIG. 21. Multiple fingers, velocity field and saturation front. Approximate analytic solution.

Figure 18 shows the evolution of the solution computed with independent random generators for each x and y column. The viscosity ratio is $\mu = 2$, so that we are well in the stable regime. (A derivation of the region of stability will be given in the next section.) Clearly the fingers introduced by the scheme are small (1 or at most 2 mesh spacing long) and have no tendency to grow. Figures 19 and 20 correspond to $\mu = 10$, for a 20×20 mesh in the unstable regime. Clearly, these fingers grow. Their growth was studied statistically in [9]. In that paper, we compute the average position of the front and the root mean square deviation of the front position from its average, both as functions of time. The results proved to be independent of mesh refinement and other factors.

We remark that the resolution at the edge of the front is nearly perfect. In Fig. 18, the resolution of the front is seen from the sharp discontinuity in s, from values at least 0.5 to the value $s \equiv 0$. In Fig. 19, the jump is from values at least 0.3 to $s \equiv 0$. See the figure legend for further discussion. Note the tendency of the velocity to avoid the trench—i.e., inverse or oil finger, and to expand at the tip of the water finger. In the stable case these tendencies are reversed.

C. *The Multiple Fingered Solution: Homogeneous Calculations*

In order to understand how multiple fingers are treated by our scheme, we consider a solution which has fingers of equal length and uniform saturation k_2 on every other Y column at time zero (see Fig. 21). We define $k_2 = k(s^*)$ where s^* is the saturation value given in Fig. 16. This value depends only on μ. Physically this means that instead of pure water (which tends to mix—macroscopically—with oil), we pump in a mixture of oil and water which has no tendency to mix further with oil.

We will compute analytically the solution using reasonable approximations, and compare it with the numerical solution. We assume that the velocity field is vertical. This is inaccurate only near the tips of the fingers.

In the pure oil region corresponding to mobility $k_1 = k$ $(s = 0)$, the vertical velocity is a constant w_3 for points above the tip of the fingers (at position y), and another

TABLE I

Length of Multiple Fingers vs Time

Time	Analytic 5 fingers	30×30 mesh 5 fingers	20×20 mesh 10 fingers	20×20 mesh 5 fingers	10×10 mesh 5 fingers
0.00	0.300	0.300	0.30	0.30	0.3
0.25	0.367	0.333	0.35	0.35	0.3
0.50	0.434	0.433	0.40	0.40	0.4
0.75	0.502	0.500	0.50	0.50	0.4
1.00	0.571	0.566	0.50	0.50	0.5
1.25	0.641	0.633	0.55	0.55	0.6
1.50	0.712	0.700	0.65	0.65	0.6
1.75	0.783	0.766	0.75	0.75	0.6
2.00	0.856	0.833	0.80	0.80	0.7

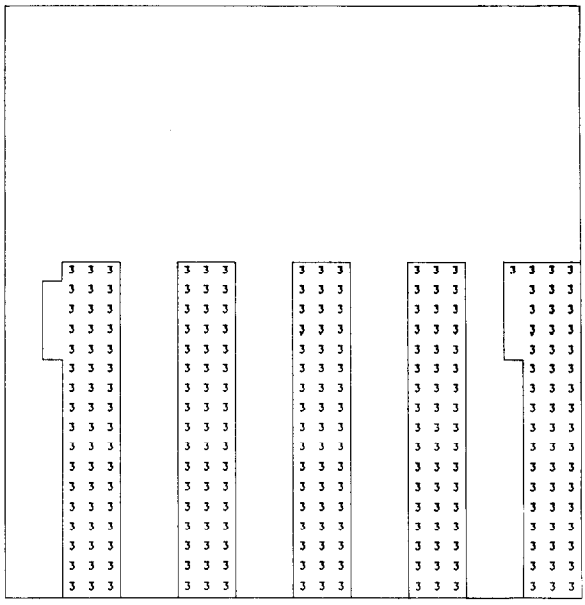

FIG. 22. Multiple fingers. Saturation values at $t = 1$ for computed solution. Cauchy data have five fingers with finger height $y = 0.3$.

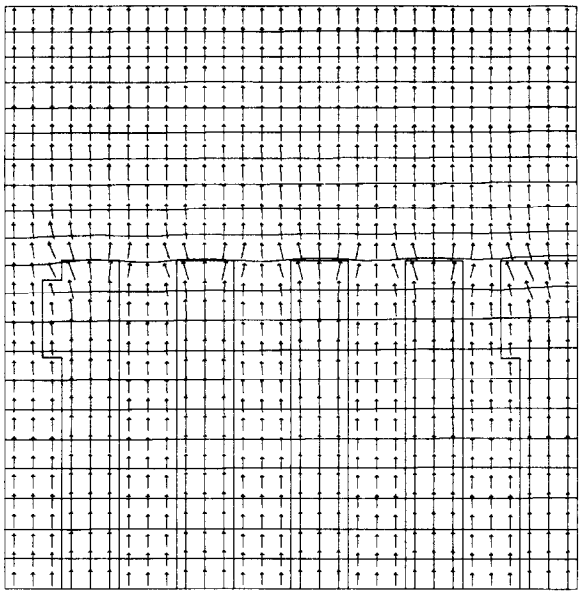

FIG. 23. Pressure contour lines and velocity field for Fig. 22. This figure justifies the assumptions used to compute the analytic solution.

constant w_1 between the fingers (see Fig. 21). Inside each finger the uniform velocity is w_2 and the saturation is k_2.

We introduce the notation $(0, E) \equiv \mathbf{E} = -\nabla p$. Since curl $\mathbf{E} = 0$, a computation of the circulation of $\mathbf{E}$ in the rectangle S in Fig. 21, yields the equality $E_1 = E_2$. Since $w_1 = k_1 E_1$, $w_2 = k_2 E_2$ we have $w_1/w_2 = k_1/k_2$, that is, the ratio of the velocities inside and outside of fingers (side by side in Fig. 21) is the mobility ratio. A discussion of related but distinct definitions of mobility ratio can be found in [4, 16]. We set $M = w_1/w_2$.

For $\mu = 2$, solution of the Riemann problem leads to $s_2 = s^* = 0.577$ and $M = 0.845$. Similarly for $\mu = 3$ we have $M = 1.0$ and for $\mu = 4$ we have $M = 1.1056$, suggesting that $\mu = 2$ is stable and $\mu = 4$ is unstable.

Since $\nabla \cdot \mathbf{v} = 0$, a flux calculation yields $2w_3 = w_1 + w_2$. Using (1.6) and computing the line integral of ∇p from 0 to Y we obtain $-vY = p(Y) - p(0) = p(Y) - p(y) + p(y) - p(0) = -E_3(Y - y) - E_2 y$. Now we substitute E_2, E_3 in terms of k_1, k_2, w_2 and solve for w_2. Since the front advances with speed $dy/dt = w_2 f'(s^*)$, an integration yields:

$$y = (\beta - ((\beta - \alpha y_0)^2 - 2\alpha\gamma t)^{1/2})/\alpha,$$

where $\alpha = (k_2 - k_1)/2k_1$, $\beta = Y(k_2 + k_1)/2k_1$, $\gamma = k_2 vYf'(s^*)$ and $y_0 = y(0)$.

We compute $y(t)$ for $\mu = 10$ and $y(0) = 0.3$ in a square domain with $Y = 1$ and $v = 1$.

In Table I, we show the "exact" $y(t)$ and the $y(t)$ computed for a variety of mesh spacings. In view of the first order accuracy of the scheme, the agreement is very good. In Figs. 22 and 23 we show the solution at time 1.0.

APPENDIX: The Accelerated Conjugate Gradient Algorithm

The problem is to solve iteratively the linear system $Mu = c$, where the matrix M is positive definite and symmetric. The standard conjugate gradient algorithm is the one described below, provided we replace N by the identity operator. See [12]. The conjugate gradient algorithm converges faster, the closer M is to the identity matrix. In order to derive the accelerated conjugate gradient algorithm we replace the original system by $(N^{-1/2}MN^{-1/2})v = N^{-1/2}c$, where $v = N^{+1/2}u$. Here N is an approximation of the matrix M. The preconditioning operator N is assumed to be symmetric and positive definite and to have a computationally inexpensive inverse.

Given u_0, an initial guess of the solution, we define $r_0 = c - Mu_0$, $p_0 = N^{-1}r_0$. The iterative procedure for $k = 0, 1, 2, \ldots$ is the following:

$$\alpha_k = \langle r_k, N^{-1}r_k \rangle / \langle p_k, Mp_k \rangle,$$

$$u_{k+1} = u_k + \alpha_k p_k,$$

$$r_{k+1} = r_k - \alpha_k Mp_k,$$

$$\beta_k = \langle r_{k+1}, N^{-1} r_{k+1} \rangle / \langle r_k N^{-1} r_k \rangle,$$

$$p_{k+1} = N^{-1} r_{k+1} + \beta_k p_k.$$

This procedure is stopped when $\langle r_k, N^{-1} r_k \rangle$ has decreased enough, and u_k is then the approximate solution of $Mu = c$.

REFERENCES

1. N. ALBRIGHT, P. CONCUS, AND W. PROSKUROWSKI, "Numerical Solution of the Multidimensional Buckley–Leverett Equation by a Sampling Method," presented at the Society of Petroleum Engineers 5th Symposium on Reservoir Simulation, Denver, Colorado, 1979.
2. A. CHORIN, *J. Comput. Phys.* **22** (1979), 517.
3. P. COLLELA, "An Analysis of the Effect of Operator Splitting and of the Sampling Procedure on the Accuracy of Glimm's Method," University of California Thesis, Berkeley, 1979.
4. F. CRAIG, "The Reservoir Engineering Aspects of Water Flooding," Society of Petroleum Engineers of AIME, Dallas, 1971.
5. P. CONCUS AND W. PROSKUROWSKI, *J. Comput. Phys.*, to appear.
6. L. DAKE, "Fundamentals of Reservoir Engineering," Elsevier, Amsterdam/New York, 1978.
7. J. GLIMM, *Comm. Pure Appl. Math.* **18** (1965), 697.
8. J. GLIMM, D. MARCHESIN, AND O. MCBRYAN, *J. Comput. Phys.* **37** (1980), 336.
9. J. GLIMM, D. MARCHESIN, AND O. MCBRYAN, *Comm. Math. Phys.* **74** (1980), 1.
10. J. GLIMM, D. MARCHESIN, AND O. MCBRYAN, *Comm. Pure and Appl. Math.*, in press.
11. T. NISHIDA, "Nonlinear Hyperbolic Equations and Related Topics in Fluid Dynamics," Publications Mathématiques D'Orsay (Université de Paris-Sud, Département de Mathématique), Orsay, France.
12. PAIGE AND SAUNDERS, *SIAM J. Numer. Anal.* **12** (1975), 617.
13. D. PEACEMAN AND H. RACHFORD, *J. Soc. Pet. Eng.* (Dec. 1962), 327.
14. D. PEACEMAN AND H. RACHFORD, *J. Soc. Ind. Appl. Math.* **3** (1955), 28–41.
15. D. PEACEMAN, "Fundamentals of Numerical Reservoir Simulation," Elsevier, Amsterdam/New York, 1977.
16. A. SCHEIDEGGER, "The Physics of Flow through Porous Media," Univ. of Toronto Press, Toronto, 1974.
17. W. G. STRANG AND FIX, "An Analysis of the Finite Element Method," Prentice–Hall, New York, 1973.
18. W. G. STRANG, On the construction and comparison of difference schemes, *SIAM J. Numer. Anal.* **5** (1968), 506.
19. J. GLIMM, E. ISAACSON, D. MARCHESIN, AND O. MCBRYAN, *Adv. Appl. Math.*, in press.